

## Piez spectroscopy of GaAs-AlAs superlattices

P. Lefebvre, B. Gil, and H. Mathieu

*Groupe d'Etudes des Semiconducteurs, Université des Sciences et Techniques du Languedoc, place Eugène Bataillon, 34060 Montpellier CEDEX, France*

R. Planel

*Laboratoire de Microstructures et Microélectronique, Centre National de la Recherche Scientifique, 196 avenue Henri Ravera, 92260 Bagneux CEDEX, France*

(Received 6 March 1989)

Piez spectroscopic studies of type-I and type-II GaAs-AlAs superlattices have been made for stress lying along the plane or along the growth axis. Ground and excited states have been studied by means of reflectivity for type-I superlattices. In type-II superlattices the  $X$  symmetry of the conduction subband has been observed. A reversal of the ordering of the  $X_z$ - and  $X_{x,y}$ -type conduction subband has been found to appear when the thickness of the AlAs slab is changed. This was interpreted as a contribution of the internal strain experienced by the AlAs slabs lattice matched to the GaAs substrate. Stress-induced switching of ordering between  $X_z$  and  $X_{x,y}$  conduction states was observed in the case of stress perpendicular to the growth axis of the superlattice. We deduce the tetragonal shear deformation potential of AlAs conduction band:  $E_2 = 5.1 \pm 0.7$  eV.

### I. INTRODUCTION

Uniaxial stress has been extensively used for investigating the intimate symmetry of the band structure of most semiconductors. In addition to this, it can also give valuable information concerning impurities through piezo-spectroscopic studies of bound excitons. Its field of application has been recently extended, with success, to heterostructure physics, as a perturbation complementary to high hydrostatic pressure.<sup>1,2</sup> These two types of perturbation can be tuned, nearly at the will of the experimentalist; this is fruitful for studying the electronic properties of heterostructures grown from lattice-mismatched bulk compounds. Moreover, the orientation of the applied stress can be chosen parallel or perpendicular to the growth axis. Then, depending on the relative orientation of the heterostructure potential and the strain Hamiltonian, peculiar couplings can be predicted theoretically between the electronic subbands, and selective dependences with the stress have been calculated for the optical transitions.<sup>3-8</sup>

Experimental investigations have been made for GaAs-Ga<sub>1-x</sub>Al<sub>x</sub>As quantum wells<sup>5,6</sup> and a reasonable agreement between theory and experiments has been obtained.<sup>2,5,6,8</sup> The case of GaAs-AlAs short-period superlattices (SPSL's) has not, to the best of our knowledge, been the subject of detailed study, when uniaxial stress is used as a mechanical perturbation.<sup>9,10</sup> Due to the relative ordering of the  $\Gamma_6^c$  and  $X_6^c$  extrema of GaAs and AlAs conduction bands, together with the value of the  $\Gamma_8^v$  valence-band offset, both type-I and type-II SPSL's can be grown as a function of  $\bar{x}$ , the thickness of the AlAs slab measured in units of the SPSL's period  $P$ .<sup>11</sup> The critical value  $\bar{x}_c$  for the type-I-type-II transition has been proposed as a function of  $P$ , using a set of proper band parameters characteristic of the two binary com-

pounds.<sup>11,12</sup> In the case of type-II SPSL's, the barrier material is AlAs for the hole and GaAs for the electron. At the type-I-type-II transition, the lowest conduction band changes its character from  $\Gamma$  to  $X$  and the SPSL becomes "indirect" or "pseudodirect".<sup>11-18</sup> Some typical properties have been reported in the recent literature; they concern the influence of an electric field applied along the SPSL axis. Danan *et al.* reported the appearance of a new luminescence line simultaneously with the disappearance of the indirect luminescence band.<sup>19</sup> In their sample, this new luminescence band was strongly coupled to the electric field; the standard indirect band was not. On the other hand, Meynadier *et al.*<sup>20</sup> studied the electric-field-induced coupling between  $X$  and  $\Gamma$  conduction bands. Their indirect transition was coupled to the electric field. The question of the identification of the symmetry of the lowest conduction band, as a function of the type-II SPSL parameters, is then opened. It is far from being recognized from the theoretical side since the predictions of numerical calculations are a sensitive function of the method used to calculate the superlattice band structure.<sup>11-18</sup> Experimental investigations are desirable to clarify this point. In this paper, we present the experimental contribution of uniaxial stress to this problem. We first examine type-I superlattices under [110] and [001] stress in order to show the influence of the stress orientation on the superlattice band structure and, more precisely, on valence-band states; selective dependences of the valence subbands are observed for ground and excited states, respectively, of light- and heavy-hole subbands. Moreover, given a subband, its slope is found to depend on the orientation of the stress.

Next we focus our attention on the case of type-II superlattices (SL's). The luminescence lines exhibit stress behaviors which differ when the stress is applied in the [110] or [001] direction. We first determine that the

ground state has the  $X$  symmetry. Second, we identify the symmetry of the lowest conduction state, which has been found to be of  $X_z$  or  $X_{x,y}$  symmetry, depending on the parameters of the superlattice. This has been interpreted, taking into account the  $\sim 14$ -meV splitting between  $X_z$  and  $X_{x,y}$  conduction minima in AlAs slabs strained by lattice matching to the GaAs substrate. The nonlinearity of the stress dependence of some electronic states suggests an identification of the transition lines in terms of recombination of localized excitons. The  $X$ -related shear deformation potential  $E_2$  is estimated at  $5.1 \pm 0.7$  eV for the AlAs conduction band.

## II. EXPERIMENTAL SETUP

The luminescence pumped by the 514.5-nm line of an ionized-argon laser was detected behind a Jobin Yvon 1.5-m-focal-length spectrometer, using a GaAs:Ce-cooled photomultiplier and a lock-in amplifier. The two types of pressure cells used along this work are presented in Fig. 1. For the in-plane stress, the sample (of typical dimensions  $8 \times 1.3 \times 0.3$  mm<sup>3</sup>) was wedged between two iron plugs. In the case of stress parallel to the growth axis, we have modified our usual cell: the sample was wedged between the iron plug and a thick sapphire window. Both incident and emitted photons needed to be reflected by a 45° mirror that was attached at the bottom of the stress system; the typical size of the sample was  $1 \times 1 \times 0.3$  mm<sup>3</sup>. In both cases, we measured the force transmitted to a quartz device, using an appropriate charge amplifier. Another type of cell has been specially designed for in-axis applied-stress experiments.<sup>21</sup> Six samples were examined in that work: three type-I superlattices and three type-II superlattices; their characteristics are summarized in Table I.

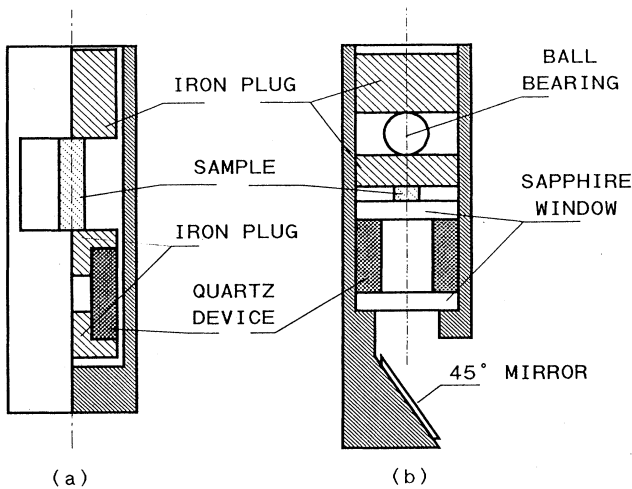


FIG. 1. Schematic view of the modifications (b), performed on a common uniaxial-stress cell (a), in order to allow on-axis uniaxial-stress experiments on thin-layer samples. In both cases, the stress is transmitted to the upper iron plug from the top to the bottom of the cryostat by a rod, and it is measured using a quartz device.

TABLE I. Relevant characteristics of the samples.  $\bar{x}$  is the thickness of the AlAs layer relative to the period of the superlattice  $P$ .

Sample no.	Period $P$ (nm)	$\bar{x}$
1	19.7	0.12
2	10.2	0.54
3	10.2	0.12
4	4.34	0.6
5	9.5	0.65
6	1	0.6

## III. TYPE-I SUPERLATTICES

We present in this section the experimental results obtained at liquid-helium temperature on type-I GaAs-AlAs superlattices, grown along the [001] direction, which we will hereafter call the  $z$  axis. We report the observed behavior of such structures under [110]-oriented uniaxial stress and, for the first time, under [001]-oriented uniaxial stress. Our experimental findings are analyzed through a simple, parameter-free model.

### A. Experimental data

Figure 2 displays the changes in the reflectance spectrum of a large-period sample ( $P=19.7$  nm and  $\bar{x}=0.12$ ) under several magnitudes of the applied [110] uniaxial

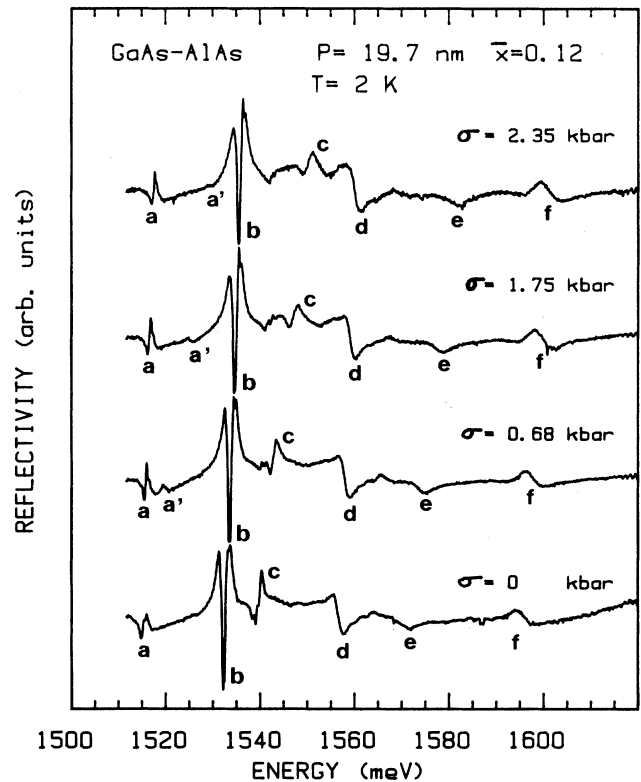


FIG. 2. Reflectivity spectrum of sample 1 under four different magnitudes of the applied [110] stress. The identification of the different structures is addressed in the text.

stress, in the energy range of interband transitions, which are labeled  $b-f$ . Notice the presence of many transitions, corresponding to excited electronic states of the SPSL. This is a great advantage of reflectance measurements, which allow a simple, direct observation of several excited intrinsic transitions in quantum wells and superlattices. As the stress is applied, the rather constant width of the reflectance structures testifies to the homogeneity of the strain over the sample. Also notice that we can observe the stress-induced splitting of the upper valence bands of the GaAs buffer layer. Thus, we can estimate the stress within an uncertainty lesser than 80 bars, by comparing the measured shifts and splitting of the  $|\frac{3}{2}, \pm\frac{3}{2}\rangle$  and  $|\frac{3}{2}, \pm\frac{1}{2}\rangle$  states of bulk GaAs to the results of Chandrasekhar *et al.*<sup>22</sup> The observed SPSL transitions were identified using a zero-stress calculation of the electronic subbands in the superlattice within the framework of the envelope-function approach of Bastard.<sup>23</sup> We took the various parameters gathered in Table II and assumed a value of the effective Rydberg equal to that of bulk GaAs (4 meV). This allows us to identify without ambiguity the  $b$ ,  $c$ ,  $d$ , and  $e$  structures of Fig. 2 as the  $e(1)$ -HH(1),  $e(1)$ -LH(1),  $e(1)$ -HH(3), and  $e(1)$ -LH(2) transitions, respectively. Note the weakness of the  $e$  transition which confirms our calculation, the  $e(1)$ -LH(2) transition being forbidden because of parity criteria. Also notice that the  $e(1)$ -HH(2) is almost unobservable because of its weakness and position [near the  $e(1)$ -LH(1)]. On the contrary, the  $e(1)$ -HH(3) structure is expected to be enhanced by the strong joint density of states of the superlattice (near the  $\Gamma$  point of the Brillouin zone), between the first conduction subband and the third heavy-hole one. This is due to the strong so-called

TABLE II. Physical constants used in this work.

	GaAs	AlAs
$\gamma_1$	6.85	3.45
$\gamma_2$	2.1	0.68
$m_e^*$	0.067	0.15
$m_{\Gamma}^{[001]}$	1.3	1.1
$m_{\Gamma}^{[001]}$	0.23	0.19
$E_g$ (meV)	1519	3130
$\frac{\partial E(\Gamma_8^v-\Gamma_6^c)}{\partial p}$ (meV/kbar)	10.7	9.9
$\frac{\partial E(\Gamma_8^v-\Gamma_6^c)}{\partial p}$ (meV/kbar)	-1.3	-1.8
$\frac{\partial E(\Gamma_8^v-\Gamma_6^c)}{\partial p}$ (meV/kbar)	5.5	5.5
$S_{11}$ ( $10^{-6}$ bars $^{-1}$ )	1.16	1.20
$S_{12}$ ( $10^{-6}$ bars $^{-1}$ )	-0.37	-0.39
$S_{44}$ ( $10^{-6}$ bars $^{-1}$ )	1.67	1.7
$a$ ( $\text{\AA}$ )	5.6533	5.6611
$b$ (eV)	-1.76	-1.76
$d$ (eV)	-4.55	-4.55
$E_2$ (eV)	$6.5 \pm 1$	$5.0 \pm 0.5$
$E_3$ (eV)	$14.5 \pm 1.5$	

valence-band mixing in the  $(k_x, k_y)$  plane which causes the HH(3) subband dispersion to be parallel to the one of the  $e(1)$  subband, near  $k=0$ . Mass mismatch effects between electron and hole probably contribute too.<sup>24</sup> The identification of the structure labeled  $f$  on our spectra is more difficult, but its strength, width, and stress-induced shift permit us to attribute it to the  $e(2)$ -HH(2) transition. The chart of the transition energies versus [110] stress is

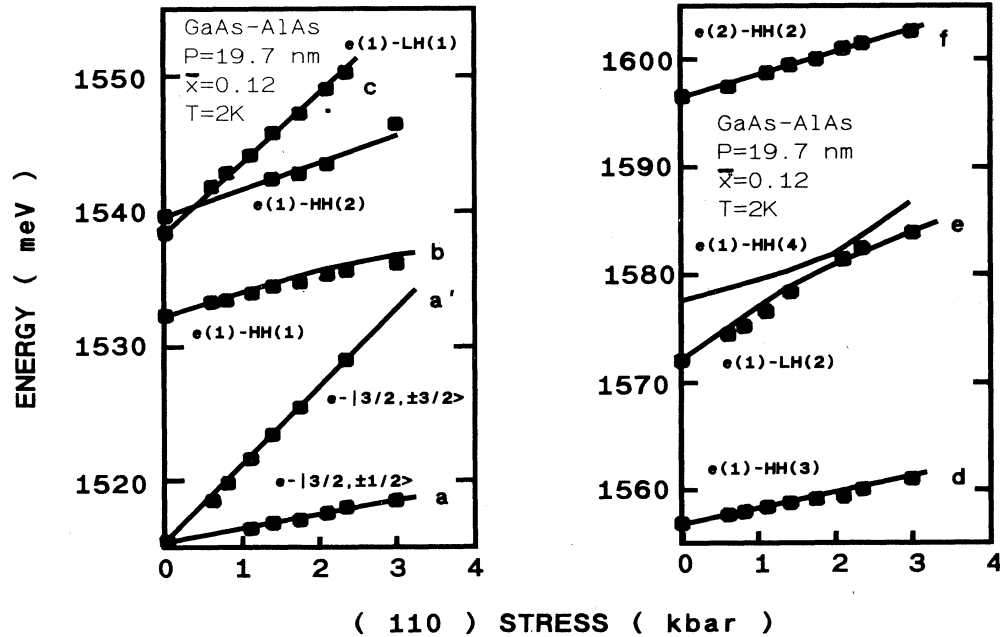


FIG. 3. Plot of the measured transition energies vs the [110] stress, in the case of sample 1. The lines through the experimental points are the result of our theoretical calculation. The identification proposed on the left part of the figure are only reliable *stricto sensu* at  $\sigma=0$  since the valence-band states can be mixed by the [110] stress.

represented in Fig. 3. The lines through the data are the result of our calculation detailed below (Sec. III B). As already observed,<sup>1,2</sup> and theoretically explained,<sup>1,2,4,5</sup> in the case of GaAs-Ga<sub>1-x</sub>Al<sub>x</sub>As quantum wells, the  $e(i)HH(j)$  transitions shift toward higher energies in a linear or slightly sublinear way, with slopes of the order of the  $e-|\frac{3}{2}, \pm\frac{1}{2}\rangle$  one in bulk GaAs ( $\sim 1$  meV/kbar). On the other hand, the  $e(i)-LH(j)$  energy shifts appear closer to the one of bulk-GaAs  $e-|\frac{3}{2}, \pm\frac{3}{2}\rangle$  transition. This "slope reversal" between the bulk-GaAs case and the superlattice one can be explained in terms of inter-valence-subband mixings produced by the crossed configuration of the strain field (along [110]) and the size-quantization axis (along [001]). We have performed the same experiment on sample 2, with thinner GaAs slabs. Only the  $e(1)-HH(1)$  and  $e(1)-LH(1)$  transitions could clearly be observed. The results are presented in Fig. 4. Higher stresses could be reached in this case before the sample breaks. The  $e(1)-HH(1)$  transitions presents a larger slope than in the previous case, while the opposite occurs for the  $e(1)-LH(1)$  transition. This is consistent with previous results on GaAs-Ga<sub>1-x</sub>Al<sub>x</sub>As quantum wells.<sup>1,2</sup>

Applying the uniaxial stress along the growth axis  $z$  is a key point for our study of type-II SPSL. To test the quality of our setup, we did preliminary experiments on type-I direct structures. Since the optical access was rather inconvenient for reflectance experiments, we could only perform luminescence and thus measure the stress-induced energy shift of the  $e(1)-HH(1)$  fundamental recombination. Figure 5 shows the result obtained for such a test sample with  $P=10.2$  nm and  $\bar{x}=0.12$  (sample 3). We have experimentally verified the behavior expected from (Refs. 3 and 4): as the size quantization and strain fields now have the same direction, the stress-induced energy shift of the  $e(1)-HH(1)$  transition is close

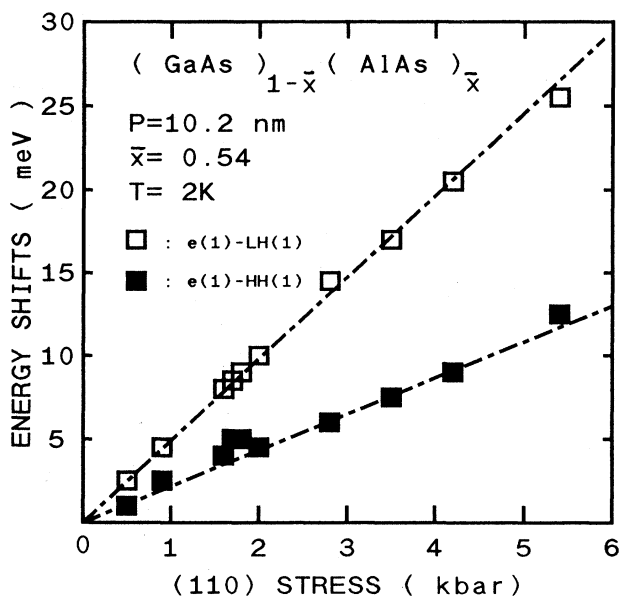


FIG. 4. The same as Fig. 2, in the case of sample 2, for the  $e(1)-LH(1)$  transition (open squares) and  $e(1)-HH(1)$  one (solid squares).

to the one of the bulk-GaAs  $e-|\frac{3}{2}, \pm\frac{3}{2}\rangle$  transition. Moreover, this is a proof of the quality of our setup, the stress being properly applied and measured, which is the main difficulty in this type of investigation.

## B. Data analysis

Our theoretical analysis has been performed as follows: we first make an envelope-function description<sup>23</sup> of the quantized levels in the superlattice at zero stress. Thus, we can make a first identification of the structures observed at zero stress. Then, the behavior of the spectra under uniaxial stress allows us to check or improve this identification because of the different pressure coefficients of light- and heavy-hole-related transitions.

We first consider the simpler case of applied stress  $\sigma$  along the [001] direction, where the symmetry of the problem is not broken. We have calculated the new SL band structure for each stress value, from the host-material shifted energies, and assuming a constant band-offset ratio; such an approximation has already proven to be valid in the 0–5-kbar range.<sup>2,5</sup> We have also neglected any influence of stress on the excitonic Rydberg energy. Following the notations of Pikus and Bir,<sup>25</sup> the conduction and valence energies in GaAs and AlAs shift by

$$\Delta E_c = a_i^c (S_{11} + 2S_{12}) \sigma,$$

$$\Delta E_{|3/2, \pm 3/2\rangle} = a_i^v (S_{11} + 2S_{12}) \sigma - b_i (S_{11} - S_{12}) \sigma,$$

$$\Delta E_{|3/2, \pm 1/2\rangle} = a_i^v (S_{11} + 2S_{12}) \sigma + b_i (S_{11} - S_{12}) \sigma,$$

where the elastic constants  $S_{ij}$  and deformation potentials  $a_i$  and  $b_i$  used can be obtained from Table II [the dependence of the band gap under hydrostatic pressure,  $\partial/\partial p (E_c - E_v)$ , is  $3(a^c - a^v)(S_{11} + 2S_{12})$ ], and  $\sigma$  represents the magnitude of the stress. Actually, our model thus predicts quasilinear shifts for all transitions of interest, neglecting the coupling with spin-orbit split-off states, which would only affect the light-hole-related transitions. As shown above, the result of this type of calculation is in very good agreement with our experimental data (see Fig. 5).

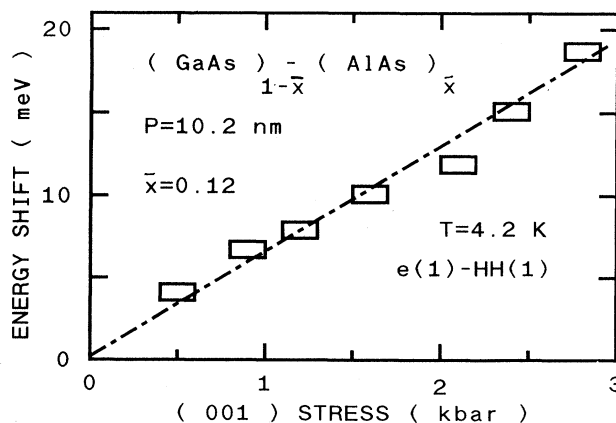


FIG. 5. Energy shift of the  $e(1)-HH(1)$  luminescence line vs the applied [001] stress, for sample 3.

In the case of an in-plane uniaxial stress, the situation is more complicated.<sup>2,4-6,8,21</sup> For a [110]-oriented stress, in the form of the Pikus-Bir Hamiltonian, extra diagonal terms proportional to the trigonal shear deformation potential  $d_i$  appear and lead to a nonlinear dependence of the valence-band splitting of both AlAs and GaAs. In the superlattice, due to the stress-induced mixing of  $|\frac{3}{2}, \pm\frac{3}{2}\rangle$  and  $|\frac{3}{2}, \pm\frac{1}{2}\rangle$  Bloch states of the binary compounds, couplings between valence subbands of so-called light- and heavy-hole type are provoked. The new eigenstates of the strained SPSL are then calculated as combinations of unstrained light- and heavy-hole states. The comparison between our calculation and experiment is shown in Figs. 3 and 4. Here, again, the agreement is very good; even though it is not as accurate as the one obtained in the case of single quantum wells, then using a variational calculation<sup>2,5</sup> it allows us to give a precise identification of the transitions. Moreover, we justify using our simple theory, which we shall do in the next section, when we subtract the valence-band-related shift from our data in order to highlight the shifts of the  $X$ -like conduction states.

#### IV. TYPE-II SUPERLATTICES

In this section, we report low-temperature photoluminescence experiments under both parallel and crossed configurations, performed on type-II SPSL's. They allowed us to investigate the symmetry properties of the  $X$ -like conduction states involved in the observed recombination lines. Three type-II SPSL's were studied; we worked in samples with constant relative thickness of AlAs  $\bar{x} \sim 0.6$  and varied the SPSL's period from 9.5 nm down to 1 nm in order to highlight typical behaviors under stress. As we shall see, the ordering of the  $X_z$ - and  $X_{x,y}$ -related subbands cannot be explained without taking into account the lattice matching of AlAs to GaAs, which produces important splittings on the conduction minima of  $X$  type, in the AlAs slabs.

##### A. Sample 4

Typical luminescence patterns collected for a type-II SL with a period of 4.34 nm with  $\bar{x}=0.6$  and in the case of [110] stress have been gathered in Fig. 6. The luminescence peaks are not symmetric with respect to their maxima; they exhibit a luminescence tail on their low-energy side. Carefully examining the shape of this transition, we could not notice any change in the line shape under stress or in the luminescence intensity, but did notice an energy shift of the peak extremum. The constant half-width of  $\sim 8$  meV testifies to a stress inhomogeneity of  $\sim 120$  bars. In Fig. 7 the shift of the luminescence energy as a function of the stress (open circles) has been plotted. From its nonlinear dependence, two asymptotic trends can be observed: the luminescence energy tends to increase for a range of stress smaller than 500 bars, then it shifts toward low energy and a linear slope is obtained in the high-stress range. Such a behavior is completely different from the behavior previously reported for type-I heterostructures, in general,<sup>1,2</sup> and, in particular, for

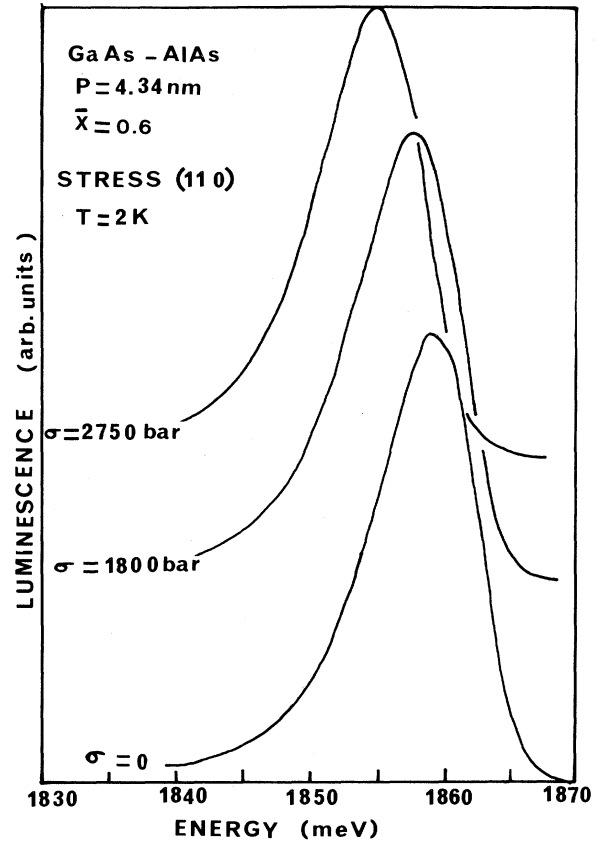


FIG. 6. Luminescence spectrum of sample 4 for three different values of the [110] stress. The energy shift of this recombination clearly shows that it does not involve  $\Gamma$ -like conduction states. This result is consistent with previous investigations on this sample (Ref. 11), where this peak was identified as the so-called "pseudodirect" transition between the first quantized subband originating from the  $X_z$  extrema of AlAs and GaAs and the first quantized subband of heavy holes.

GaAs-AlAs SL's studied in Sec. III, where the transition energy always increases with the stress due to the large widening of the  $\Gamma_8^v$ - $\Gamma_6^c$  direct band gap of the bulk host materials under the hydrostatic part of the strain field.

Such findings should be confirmed by experimental investigations when the stress is applied in another direction. This has been done. Figure 8 is the analog of Fig. 6, but now the experimental features have been collected for a [001] orientation of the external stress. The peak intensity has not been found to vary with the stress. The half-width of the transition was constant for all stresses, and once more the homogeneity of the applied strain field is very good, even at high stress. An increase of the stress leads to a decrease in the transition energy. The shift of the transition energy under stress is plotted in Fig. 9 (open circles). We first observe a small sensitivity to the applied stress up to 1.2 kbar, then it rapidly decreases and a linear slope is obtained as soon as the stress exceeds 2 kbar.

The effect of the stress on the valence-band states has

been calculated using the set of characteristic parameters gathered in Table II. The accuracy of this calculation is very good as we detailed in the first part of this work when type-I superlattices were studied. Note, however, that the hydrostatic contribution is changed between type-I and type-II situations. Subtracting the contribution of the heavy-hole subband and the hydrostatic effect (decreasing of the transition energy at rate  $-0.6$  meV/kbar) we obtain, when assuming no change in the effective Rydberg, the influence of the shear component of the strain field on the conduction level, for each situation experimentally encountered.

We now discuss the possible origin of conduction levels from the point of view of the stress experiments. The [001]-stress dependence cannot be explained with transition between  $\Gamma$  valence-band states and conduction states built from  $L_6^c$  extrema of the bulk band structure of GaAs and AlAs since the transition energy should also increase (note, however, that the increase of the  $\Gamma_8^v-L_6^c$  indirect band gaps under the hydrostatic part of the strain is commonly accepted to be about half of the increase of  $\Gamma_8^v-\Gamma_6^c$  for the bulks<sup>26-28</sup> and that the shear part of the [001] stress will not lift the fourfold degeneracy of the  $L_6^c$  extrema). On another hand, the experimental behavior is consistent with a conduction state built from  $X_6^c$  extrema of the bulk conduction states. The stress also splits the different critical points of  $X_6$  symmetry (except if it is [111] oriented) and the analysis of data is quite delicate.

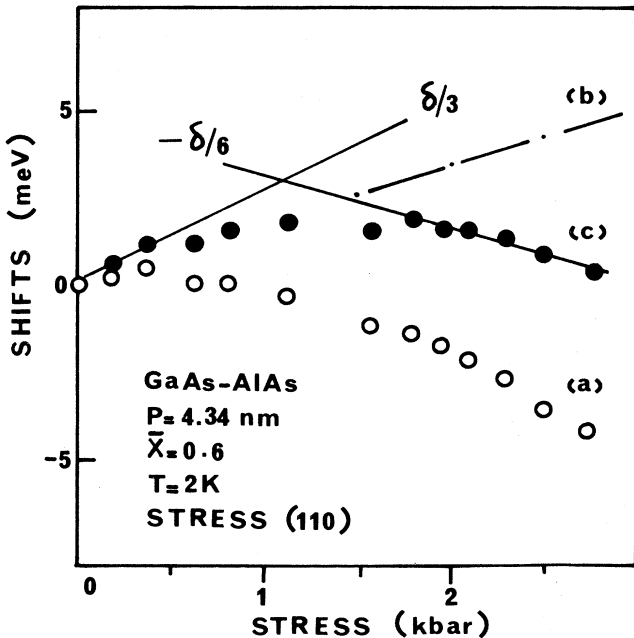


FIG. 7. The open circles, (a), represent the [110] stress-induced energy shift of the luminescence maximum of sample 4. Subtracting the hydrostatic contribution and [dashed-dotted line (b)] valence-band effect, one obtains the contribution of the only conduction band, (c), represented by solid circles. The asymptotic behaviors at low and high stress (solid lines) suggest an  $X_z$ -like character of the conduction subband near  $\sigma = 0$  and an  $X_{x,y}$ -like one for  $\sigma > 1$  kbar.

To describe the electronic structure of sample 4 we used the envelope-function approximation<sup>23</sup> around the  $X$  extremum as previously applied with success by Danan *et al.*<sup>11</sup> in their earlier work on these samples. The constants relative to  $X$  extrema are also gathered in Table II. At this stage, the splitting of AlAs  $X$  states is not taken into account. To account for the influence of the stress on the valence-band states, we adopt the procedure used for the type-I situation. We first neglect any influence of the uniaxial stress on the valence-band offset and only treat the influence of the shear part of the strain field on the splitting of the valence subbands.

Concerning the hydrostatic shift for  $\Gamma_8^v-X_6^c$  indirect transitions, it is now well established from both the experimental<sup>28-32</sup> and theoretical sides<sup>33,34</sup> that the corresponding hydrostatic deformation potential ( $E_1$ ) is 1 order of magnitude smaller than that of  $\Gamma_8^v-\Gamma_6^c$ , with opposite sign. Although this quantity is now quite well known for GaAs,<sup>28-32</sup> AlAs has not been the subject of so many studies. Hydrostatic-pressure measurements suggest  $dE_{g_x}/dP \sim -1.8$  meV/kbar.<sup>35</sup> Here for uniaxial stress  $dE_{g_x}/d\sigma$  is 3 times smaller. Let us now consider the  $X_6^c$  conduction states under the shear part of the uniaxial stress: to express the influence of the stress on electron states, one has to recall earlier works devoted to many-valley semiconductors. Under uniaxial [001] and [110] compressions, the degeneracy of the three equivalent  $X_6^c$

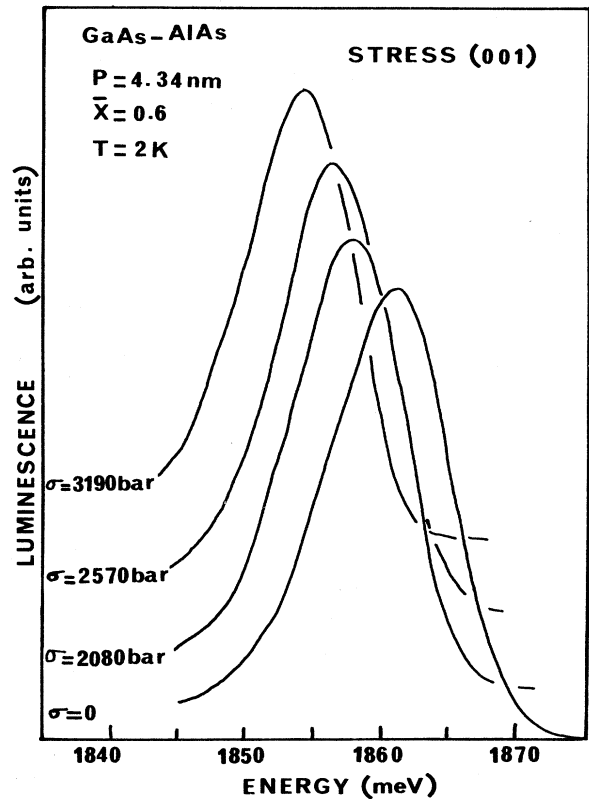


FIG. 8. The analog of Fig. 6, in the case of a [001] stress. Such a behavior confirms that the luminescence process does not involve  $\Gamma$ -like conduction states.

minima is lifted. In the notation of Brooks,<sup>36</sup> the inter-band splitting is given by

$$S = E_2 \mathbf{n} [\vec{\mathbf{e}} - \frac{1}{3}(e_{xx} + e_{yy} + e_{zz})\vec{\mathbf{1}}] \cdot \mathbf{n},$$

where  $\mathbf{n}$  is a unit vector in the direction of the band extrema in  $\mathbf{k}$  space,  $\vec{\mathbf{1}}$  is the unit dyadic, and  $E_2$  the corresponding shear deformation potential.

Table III summarizes the values of the conduction-band shifts produced at zone boundaries, for the bulk, in the cases of [111]-, [110]-, and [001]-oriented stress. The valley splitting is  $E_2(S_{11} - S_{12})\sigma$  for [001] stress and half of this quantity for [110] stress, and with opposite sign. Moreover, under [001] stress, the  $X_z$  valley is pushed toward low energy, in contrast to [110] stress, for which it is the case of  $X_x$  and  $X_y$  valleys.

On the other hand, taking into account the anisotropy of the  $X_6^c$  valleys for the two binary compounds GaAs and AlAs, a splitting of SL energy levels associated with  $X$  minima occurs in zero stress due to mass anisotropy:<sup>11</sup> the lowest-energy subbands are derived from  $X_z$  (the quantization mass (the [001] mass) is the longitudinal mass  $m_l$ , heavier than the transverse mass  $m_t$ , which is relevant for the quantization of  $X_x$ - and  $X_y$ -related SL states).

Taking into account the zero-stress ordering of levels

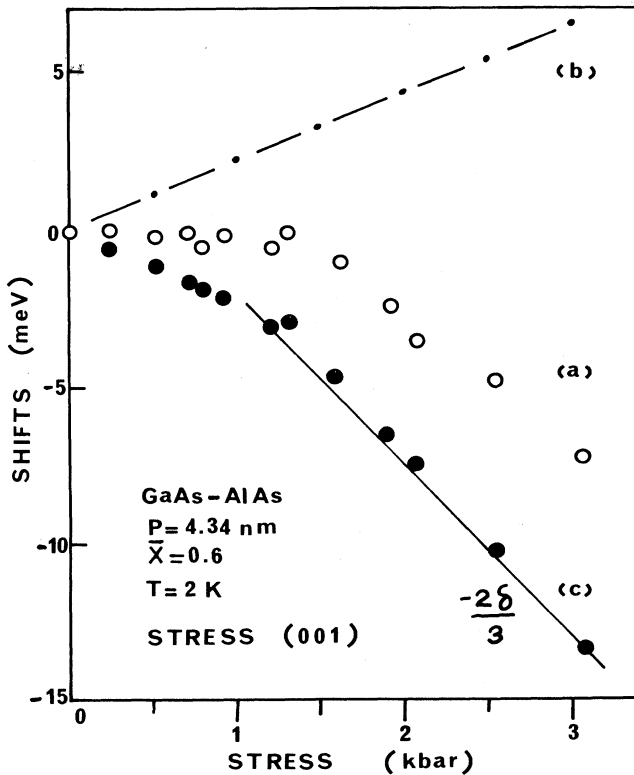


FIG. 9. The same as Fig. 7 for an applied [001] uniaxial stress. Here, the energy shift of conduction states is merely negative. A slight nonlinearity suggests a recombination process involving localized potentials. The valence-band and hydrostatic contributions are represented by the dashed-dotted line, (b). The solid line represents the shift of  $X_z$  conduction state.

TABLE III. Stress-induced splittings of conduction states  $\delta = -E_2(S_{11} - S_{12})\sigma$ ,  $\omega = -E_3(S_{44}/9)\sigma$ ,  $\xi = E_1^x[(S_{11} + 2S_{12})\sigma/3]$ , and  $\lambda = E_1^l[(S_{11} + 2S_{12})\sigma/3]$ .  $\sigma$  is negative for a compressive stress.

Valley	Stress		
	[001]	[110]	[111]
$X_z$	$\xi - 2\delta/3$	$\xi + \delta/3$	$\xi$
$X_x$	$\xi + \delta/3$	$\xi - \delta/6$	$\xi$
$X_y$	$\xi + \delta/3$	$\xi - \delta/6$	$\xi$
$L_{\langle 111 \rangle}$	$\lambda$	$\lambda - 3\omega/2$	$\lambda - 3\omega$
$L_{\langle 111 \rangle}$	$\lambda$	$\lambda + 3\omega/2$	$\lambda + \omega$
$L_{\langle 111 \rangle}$	$\lambda$	$\lambda + 3\omega/2$	$\lambda + \omega$
$L_{\langle 111 \rangle}$	$\lambda$	$\lambda - 3/2\omega$	$\lambda + \omega$

predicted by this approach, the influence of stress is sketched in Fig. 10. Note that these schemes would look very different if  $X_{x,y}$ -like states lay under  $X_z$ -like states.

Let us first consider the [110] experiment: the valence-band contribution has been represented in Fig. 7 (dashed-dotted line), including the influence of the hydrostatic component of the strain field. The conduction contribution to the shift, deduced from each experiment has been represented with solid circles. The conduction level is measured to shift toward high energy with a slope of  $\sim 2.7$  meV/kbar, then the slope reduces, and, at high stress, a linear regime with a slope of  $-1.3$  meV/kbar is reached. We first note the asymptotic tendency to match with the scheme of Fig. 10. This proves the  $X_z$ -like state to be the ground state. In addition, the nonlinear behavior of the electronic states results from a mixing between  $X_z$  and  $X_{x,y}$  and cannot be explained in terms of intrinsic luminescence for which linear slopes are expected. To go further we next consider the [001] experiment. The electronic contribution has been obtained in a manner similar to the case of [110] stress, *mutatis mutandis*. Once more, a weak nonlinear dependence is first obtained; then, at high stress, a constant shear slope of about  $-5.6$

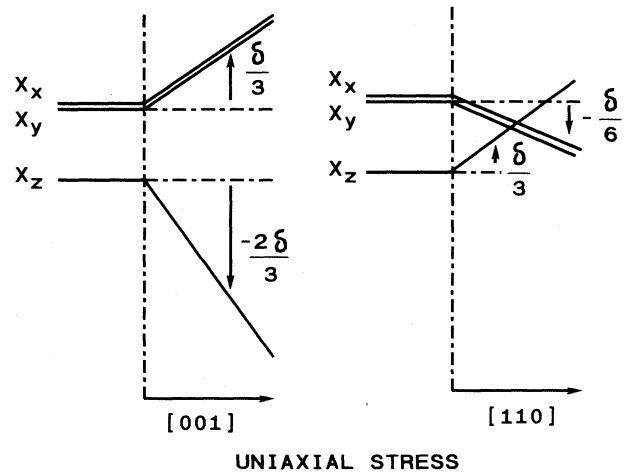


FIG. 10. Schematic behavior of the three zone-edge-related conduction subbands under both directions of the stress. The zero-stress ordering of the conduction-band minima is consistent with an "effective-mass" approach of the problem.

meV/kbar is measured. A linear dependence should be expected in the case of intrinsic luminescence. From the asymptotic cases of small and high stress, we can roughly estimate the stress splitting of  $X$  states; we obtain 4 meV/kbar for [110] stress and 8.4 for [001] stress (the theory predicts a ratio of 0.5 for these two quantities). Therefore, here we can propose an average value for  $E_z$ :  $5.5 \pm 0.3$  eV, a value to be compared with the one previously reported for bulk GaAs (6.5 eV).<sup>37</sup> We also extract from the asymptotic behaviors an estimation of the  $E_z$ - $E_{x,y}$  zero-stress splitting: 6.5 meV.

The nonlinear behaviors suggest an interpretation in terms of mixing between  $X_z$  and  $X_{x,y}$  conduction states; then the luminescence corresponds to recombination of

$$\begin{array}{c} \phi|X_z\rangle \quad \psi|X_x\rangle \quad \psi|X_y\rangle \\ \langle X_z|\phi^* \left[ \begin{array}{ccc} E_z + f_z(X) & \langle \phi|\psi\rangle\langle X_z|U|X_x\rangle & \langle \phi|\psi\rangle\langle X_z|U|X_y\rangle \\ \langle X_x|\psi^* \left[ \begin{array}{ccc} \langle \psi|\phi\rangle\langle X_x|U|X_z\rangle & E_{x,y} + f_x(X) & \langle X_z|U|X_y\rangle \\ \langle X_y|\psi^* \left[ \begin{array}{ccc} \langle \psi|\phi\rangle\langle X_y|U|X_z\rangle & \langle X_y|U|X_x\rangle & E_{x,y} + f_x(X) \end{array} \right] \end{array} \right] \end{array} \right], \end{array}$$

where  $\phi$  and  $\psi$  are the electronic envelope functions for the  $X_z$  and  $X_{x,y}$  well states, respectively, and  $f_i$  the stress shift of the confined level labeled by the Bloch wave  $|X_i\rangle$ . In the case of a spherical potential,  $\Delta = \langle X_i|U|X_j\rangle$  is the so-called valley-orbit interaction parameter.  $E_i$  represents the energy for the electron confined in an  $X_i$  conduction level, from which we subtract the effective binding energy. Due to the anisotropy of the effective mass of electrons, the binding energy is believed to depend on the  $X_i$  critical point from which the electron state presently considered is dangling.

We could fit the experiment with the following parameters:  $E_z = 5.5$  eV and an  $E_z$ - $E_{x,y}$  splitting 6.5 meV from asymptotic behaviors,  $\langle \phi|\psi\rangle = 0.94$  from calculation, and  $\Delta$  from nonlinearities. We found  $\Delta = 1.5$  meV for [110] stress and  $\Delta = 3$  meV for [001] stress. This enables us to propose a mean value  $\Delta = 2 \pm 1$  meV. The crudeness of this model cannot be ignored; The values of  $\Delta$  may be compared with valley-orbit parameters obtained for bound excitons in bulk semiconductors,  $\Delta = 4$  meV for a hydrogenic donor (S) in GaP (Ref. 40) and  $\Delta = 8$  meV for nitrogen in GaP (here the impurity potential is strongly localized in the central cell),<sup>41</sup> or with the value of the  $\Gamma$ - $X$  mixing potential (1 meV) found by Meynadier *et al.*<sup>20</sup> after performing Stark-effect investigations. The magnitude of  $\Delta$  compared with  $E_z$ - $E_{x,y}$  reveals the strong mixing of  $X_z$  and  $X_{x,y}$  produced by the localized potential.

The lattice mismatch between AlAs and GaAs (0.12%), which has not yet been taken into account, should now be considered. Assuming that the GaAs buffer imposes its lattice parameter, one can calculate the magnitude of the biaxial compressive stress experienced by the AlAs slabs:<sup>42</sup> we find  $\sim -1.7$  kbar. This stress splits the valence-band and  $X$  conduction states in AlAs. Then, we have to consider two potential wells for  $X$  electrons. Elementary calculation of the  $X$  conduction split-

ting shows that a biaxial compressive [001]-oriented stress is equivalent to a compressive [110]-oriented uniaxial stress, with a magnitude 2 times larger. The bottom of  $X_z$  ( $X_{x,y}$ ) potential wells is pushed toward high (low) energy and its depth is reduced (enhanced). Using the experimental value of conduction splittings previously obtained through the asymptotic trends under [001] and [110] stress ( $\sim 8$  meV/kbar), we can recalculate the depth of  $X_z$  and  $X_{x,y}$  potential wells and obtain a novel description of conduction states. Such a biaxial stress leads to a splitting of  $\sim 14$  meV which is in close agreement with the candidate value (19 meV) proposed in Ref. 38. The envelope-function-approximation (EFA) splitting is reduced from 48 to 34 meV. Although the calculation has been improved, we are still far from the experimental value. Nevertheless, note that the  $X$  masses near the  $X$  point of AlAs and GaAs are very poorly known quantities and that no calculation of the Rydberg or binding energy has been attempted in this work, due to the difficulty of treating such a problem when both electron and hole effective masses are anisotropic.

## B. Sample 5

A second superlattice with period 9.5 nm and  $\bar{x} = 0.65$  has also been selected for being investigated under [001] and [110] stress. We first discuss the data obtained in the case of stress lying along the [001] direction. In that case, stresses up to 1 kbar could be applied. A logarithmic plot of the luminescence patterns has been given on Fig. 11. Two different trends can be observed: First, the highest-energy transition (labeled  $e$ ), easily observable in reflectivity,<sup>43</sup> shifts toward high energy; its slope and energy position enable one to identify it as hot luminescence corresponding to recombination of direct  $e_{\Gamma(1)}$ -HH(1) type-I excitons. Second, lower in energy, one easily

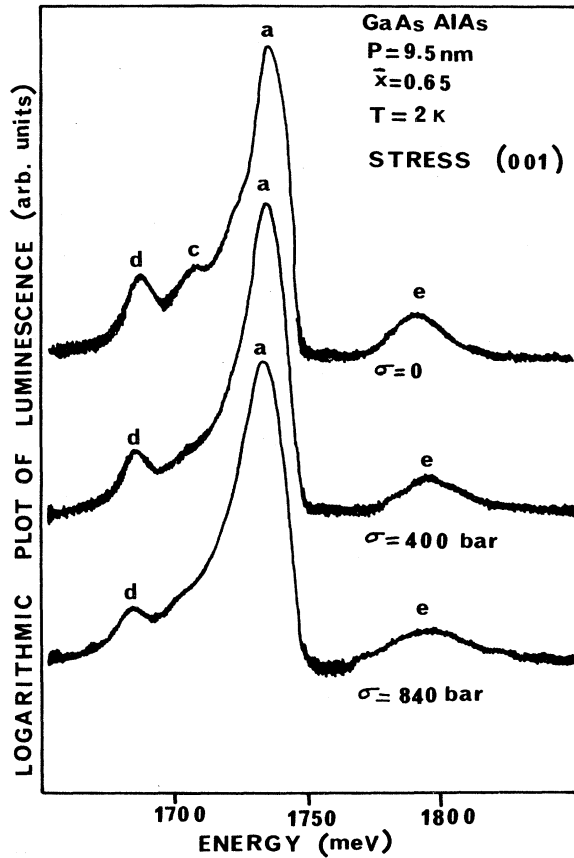


FIG. 11. Evolution of the luminescence spectrum of sample 5 under [001] stress. We chose to plot the logarithm of the luminescence intensity vs the stress. Notice that it was difficult to follow the  $b$  and  $c$  lines under stress.

resolves four transitions with negative slopes which reflect the  $X$  nature of the conduction states involved. Early on, Danan<sup>44</sup> suggested an identification of  $b, c, d$  lines in terms of phonon-assisted recombinations with three different phonon energies.

The direct luminescence shifts with a slope of  $\sim 5.7$  meV/kbar, while the  $a$  luminescence exhibits a negative linear slope of  $\sim -3$  meV/kbar. A line-shape deconvolution was made to estimate the influence of the stress on the energy splitting between  $a$  and  $b, c, d$  lines. Due to the important strength of  $a$  line, always  $\sim 10^2$  times more intense than  $b, c, d$ , and the overlap between its low-energy wing and  $b, c, d$  lines, we could not determine with precision the position of  $b$  and  $c$ , but the  $a-d$  splitting was always found to reduce when increasing the stress. Second, we analyzed the [110] experiment for which some typical luminescence spectra are displayed in Fig. 12, on a linear scale of intensities. We could obtain nicer data. At zero stress, we rediscover the luminescence spectrum dominated by the  $a$  line. The important point to outline now is the strong decrease of the intensity of the  $a$  transition when the [110] stress increases while the remaining three ( $b, c$ , and  $d$ ) keep roughly the same intensity and relative magnitude with respect to the direct luminescence.

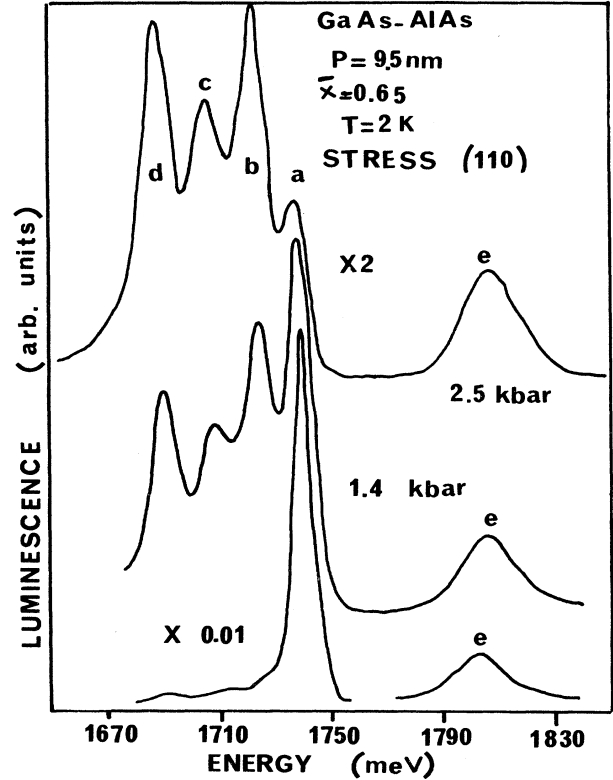


FIG. 12. Photoluminescence spectra of sample 5 under [110] uniaxial stress. The peak labeled  $a$  was previously (Ref. 44) identified as a no-phonon luminescence arising from the  $X_2$ -like “pseudodirect” recombination. Peaks  $b, c$ , and  $d$  were interpreted as phononic replicas of the  $a$  line. The fast decrease of the intensity of the  $a$  line, while the  $b, c$ , and  $d$  peaks are roughly constant, suggests that the latter ones do not have the same physical origin as the former.

Then, we could accurately measure the energy position of  $b, c, d$  lines under stress since the intensity of the  $a$  line quickly collapses and since the  $a-b, c, d$  splitting now increases with the [110] stress. The experiment is illustrated in the full diagram of energy shift given in Fig. 13. Different slopes are reported for the indirect transitions: a small negative slope for  $a$  ( $\sim -0.4$  meV/kbar) and a strong negative slope for  $b, c$ , and  $d$  ( $\sim -4.7$  meV/kbar). These [110]-stress data reveal that, although the four lines all originate from a conduction state  $X$ , they do not obey the same symmetry rules. The stress-induced splitting between all luminescence lines, together with differences between excitonic lifetimes, should dominate the magnitude of the relative intensities inside the luminescence band. Therefore, we associate the lowest-energy lines ( $b, c, d$ ) with phonon-assisted recombination of the  $(\Gamma_v-X_{x,y})$  forbidden exciton with long lifetime, while the  $a$  line (a zero-phonon line) should correspond to recombination of excitons with shorter lifetimes and with the electron wave function pinned to  $X_2$ . This confirms the observations reported in (Ref. 38). We suggest that the ordering of the conduction states is switched under stress from  $X_z-X_{x,y}$

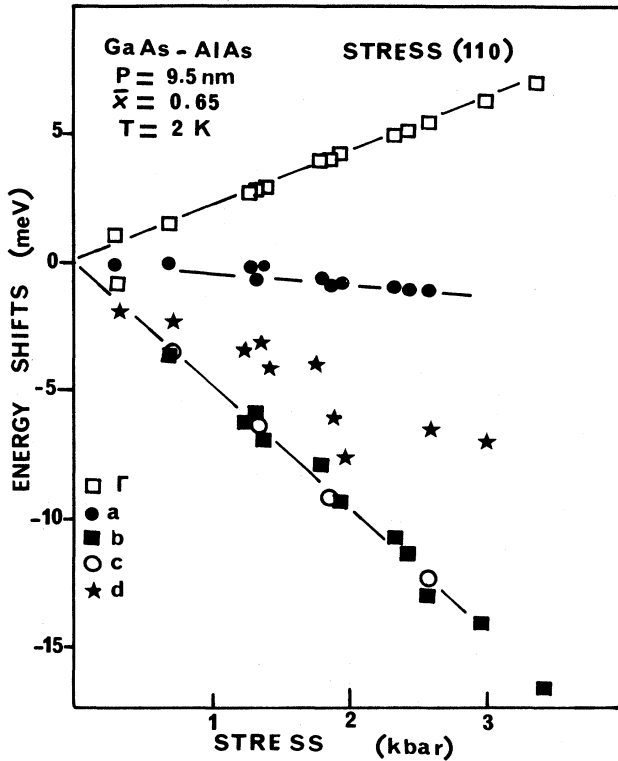


FIG. 13. Energy shifts of the five luminescence peaks of sample 5, vs the magnitude of the [110] uniaxial stress. Clearly, the shift of the  $e$  peak confirms our previous interpretation. Note that the  $b$  and  $c$  peaks shift parallelly to one another and that their slope is quite stronger than the one of the  $a$  peak. The intermediate behavior of the low-energy structure  $d$  is more difficult to address.

to  $X_{x,y}-X_z$ . Now, coming back to the [001] stress where the changes in energy ordering differ from the case of [110] stress, no drastic alteration of the shape of the luminescence spectrum is expected if the shortest recombination process corresponds to the lowest conduction state  $X_z$ , as is actually observed here.

To extract the influence of the *shear* part of the stress on the conduction states, we used the procedure described above, using the distribution of valence subbands corresponding to the case of this superlattice. The identification of all transitions in the indirect luminescence band can be made as follows: the  $a$  luminescence line is found to follow the  $X_z$  conduction subband which is then calculated to shift with a *shear* slope of  $+2.4$  meV/kbar toward high energy under [110] stress and with a *shear* slope of  $-4.7$  meV/kbar toward low energy for [001] stress. Then electron states pinned to either  $X_x$  or  $X_y$  conduction states should shift toward low energy with a *shear* slope of  $-1.2$  meV/kbar for [110] stress. This is actually deduced from the experiment for  $b$  and  $c$  transitions. Next, considering [001] stress, the  $X_x$ - or  $X_y$ -related transitions are expected to shift toward high energy with a *shear* slope half that of the  $X_z$  one and with opposite sign: this explains that the  $b$  and  $c$  lines are masked under [001] stress due to their small magnitude

compared with the  $a$  line. We experimentally estimate a shear stress splitting of  $3.6$  meV/kbar for [110] stress and of  $7$  meV/kbar for [001] stress, to which corresponds  $E_2=4.5\pm 0.5$  eV. A reversal of ordering between  $X_z$  and  $X_{x,y}$  is produced for stress smaller than 200 bars, in the case of [100] stress. At zero stress, the lowest conduction level is found to be  $X_z$  and the  $X_z-X_{x,y}$  splitting is estimated at  $\sim 1.5$  meV. This value is in the trend predicted by the EFA: taking into account the lattice mismatch, we calculate an  $E_{x,y}-E_z \sim 9$  meV.

### C. Sample 6

We now study an ultrathin short-period superlattice of period  $\sim 1$  nm with an aluminum concentration of 0.6. The luminescence is much weaker than for samples 4 and 5, and the experimental patterns consist of four main transitions which have been earlier identified as phonon replicas of the higher-energy transition (at 2096 meV at zero stress).<sup>44</sup> Under [110] stress, all these lines shift linearly and rapidly toward low energy with a slope of  $\sim -4.4$  meV/kbar. This is not the situation we observed for samples 4 and 5. Some typical luminescence spectra obtained in the range 0–5.3 kbar are displayed in Fig. 14.

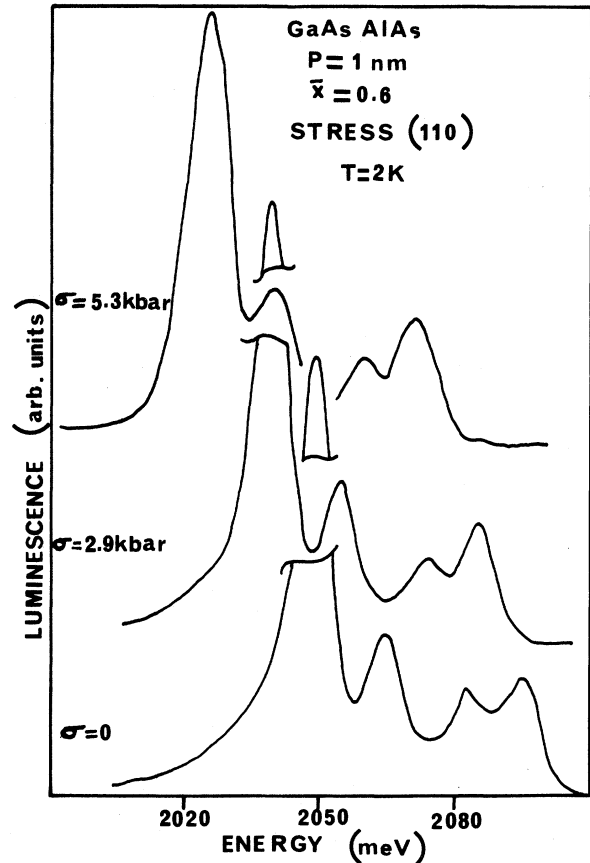


FIG. 14. Luminescence spectrum of sample 6 under [110] uniaxial stress. Here the intensities do not depend on the magnitude of the stress, and all the peaks shift toward low energy with the same important slope. This behavior should be explained by a series of phonon-assisted  $X_{x,y}$ -related recombinations.

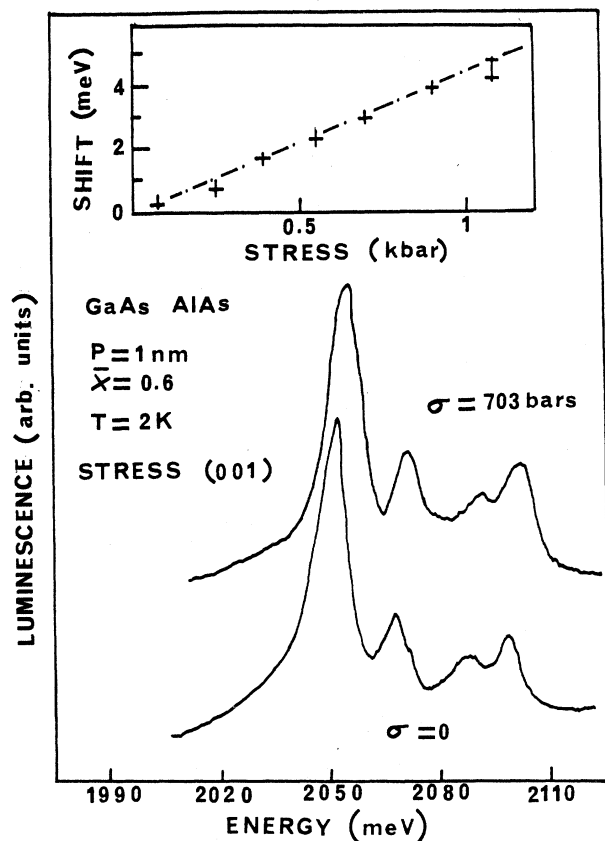


FIG. 15. The same as Fig. 14 but for [001] stress. All peaks shift toward high energy at a rate which testifies to the  $X_{x,y}$  nature of the lowest conduction band for this sample.

The whole intensity of the luminescence patterns has not been found to vary in a significant way with the magnitude of the stress. The relative intensity of each luminescence line in the series of peaks was always constant. All these data are consistent with an  $X_{x,y}$  ground state at zero stress. The [001]-stress patterns represented in Fig. 15 confirm this interpretation: the four lines shift toward high energy with the same slope of  $\sim 4.5$  meV/kbar. Performing the same treatment as in the previous section, we obtain  $\delta = 10.2$  meV/kbar from the [110]-stress experiments, while the [001]-stress one provides  $\delta = 7.2$  meV/kbar. Accounting for the elastic constant of AlAs, we thus obtain an average value of  $E_2 = 5.7 \pm 0.9$  eV. Now, coming back to the nature of the fundamental conduction state, our calculations in the EFA give an  $E_{x,y}$ - $E_z$  splitting of  $\sim 10$  meV if the lattice-mismatch effects are ignored. If they are not, we obtain an  $E_z$ - $E_{x,y}$  split-

ting of  $\sim 5$  meV, which qualitatively agrees with the experiment. Therefore, in this last case, the conduction ground state is of  $X_{x,y}$  symmetry, which can be accounted for within the EFA when considering the built in strain effects.

## V. CONCLUSION

Uniaxial-stress measurements have been made for a series of GaAs-AlAs superlattices for which both period and relative thickness of the slabs have been varied. A great variety of results was obtained. For type-I superlattices, one could clearly identify ground and excited states of light- and heavy-hole excitons. We could also demonstrate the mixing of their wave functions when an external strain field is applied. Concerning type-II superlattices, the selective dependence of all luminescence lines with the orientation of the stress enabled us to associate some transitions with  $X_z$  conduction states and others with  $X_{x,y}$  conduction states. The nature of the lowest luminescence level can be  $X_z$  or  $X_{x,y}$  depending on the superlattice parameters. Our findings closely agree with two other recent investigations by Scalbert *et al.*<sup>38</sup> (photoluminescence time-decay measurements) and van Kesteren *et al.*<sup>15</sup> (optically detected magnetic resonance). Comparison of the results obtained through these three works is strongly consistent with the notion of  $R_z$  and  $R_{x,y}$  regions introduced in Fig. 1 of Ref. 38, where the boundaries between type-I, type-II  $R_z$ , and type-II  $R_{x,y}$  regions have been plotted as a function of the relevant SPSL parameters (GaAs and AlAs layer thicknesses). Moreover, a reversal of ordering of  $X$  conducting states could be produced under stress. The nonlinear dependence of the transition lines observed in one sample has been attributed to a mixing of electron wave functions pinned to  $X_z$  and  $X_{x,y}$  minima of the conduction band produced by a localized potential. As a possible origin of such a mixing potential, one can propose interfacial states or impurities (their density may depend on growth conditions). An average value  $E_2 = 5.1 \pm 0.7$  eV is retained for the shear deformation potential of  $X$  states in AlAs. The data have been found to be roughly consistent with EFA calculations, under the condition that the biaxial compression of AlAs slabs due to the lattice mismatch between AlAs and GaAs was not ignored.

## ACKNOWLEDGMENTS

The authors wish to acknowledge G. Le Roux for x-ray diffraction analysis, and F. Mollot and C. Benoît à la Guillaume for fruitful discussions.

<sup>1</sup>C. Jagannath, E. S. Koteles, J. Lee, Y. J. Chen, B. S. Elman, and J. Y. Chi, Phys. Rev. B **34**, 7027 (1986).

<sup>2</sup>B. Gil, P. Lefebvre, H. Mathieu, G. Platero, M. Altarelli, T. Fukunaga, and H. Nakashima, Phys. Rev. B **38**, 1215 (1988).

<sup>3</sup>G. D. Sanders and Yia-Chung Chang, Phys. Rev. B **32**, 4282

(1985).

<sup>4</sup>C. Mailhot and D. L. Smith, Phys. Rev. B **36**, 2942 (1987).

<sup>5</sup>G. Platero and M. Altarelli, Phys. Rev. B **36**, 6591 (1985).

<sup>6</sup>J. Lee, C. Jagannath, M. O. Vassel, and E. S. Koteles, Phys. Rev. B **37**, 4164 (1988).

- <sup>7</sup>J. Lee and M. O. Vassel, *Phys. Rev. B* **37**, 8855 (1988); **37**, 8861 (1988).
- <sup>8</sup>R. Sooryakumar, A. Pinckzuk, A. C. Gossard, D. S. Chemla, and L. J. Sham, *Phys. Rev. Lett.* **58**, 1150 (1987).
- <sup>9</sup>B. Gil, P. Lefebvre, H. Mathieu, F. Mollot, and R. Planel, in *Proceedings of the 19th International Conference on the Physics of Semiconductors, Warsaw, 1988*, edited by W. Zawadzki (Institute of Physics, Polish Academy of Sciences, Warsaw, Poland, 1989), p. 365.
- <sup>10</sup>P. Lefebvre, B. Gil, H. Mathieu, and R. Planel, *Phys. Rev. B* **35**, 5550 (1989).
- <sup>11</sup>G. Danan, B. Etienne, F. Mollot, R. Planel, A. M. Jean Louis, F. Alexandre, B. Jusserant, G. Le Roux, J. Y. Marzin, H. Savary, and B. Sermage, *Phys. Rev. B* **35**, 6207 (1987), and references therein.
- <sup>12</sup>D. Z. Y. Ting and Yia-Chung Chang, *Phys. Rev. B* **36**, 1359 (1987), and references therein.
- <sup>13</sup>E. Finkman, M. D. Sturge, M. H. Meynadier, R. E. Nahory, M. C. Tamargo, D. M. Huang, and C. C. Chang, *J. Lumin.* **39**, 57 (1987).
- <sup>14</sup>B. A. Wilson, *IEEE J. Quantum Electron.* **QE-24**, 1763 (1986).
- <sup>15</sup>H. W. van Kesteren, E. C. Cosman, P. Dawson, K. J. Moore, and C. T. Foxon, *Phys. Rev. B* **39**, 13 426 (1989).
- <sup>16</sup>J. Ihm, *Appl. Phys. Lett.* **50**, 1068 (1988).
- <sup>17</sup>D. M. Wood, S. H. Wei, and A. Zunger, *Phys. Rev. B* **37**, 1342 (1988).
- <sup>18</sup>M. Alouani, S. Gopalan, M. Garriga, and N. E. Christensen, *Phys. Rev. Lett.* **61**, 1643 (1988).
- <sup>19</sup>G. Danan, F. R. Ladan, F. Mollot, and R. Planel, *Appl. Phys. Lett.* **51**, 1605 (1987).
- <sup>20</sup>M. H. Meynadier, R. E. Nahory, J. M. Worlock, M. C. Tamargo, J. L. de Miguel, and M. D. Sturge, *Phys. Rev. Lett.* **60**, 13 (1988).
- <sup>21</sup>R. Sooryakumar, *Comments Condensed Mater. Phys.* **14**, 43 (1988).
- <sup>22</sup>M. Chandrasekhar and F. M. Pollak, *Phys. Rev. B* **15**, 2127 (1977).
- <sup>23</sup>G. Bastard, *Phys. Rev. B* **25**, 7584 (1982).
- <sup>24</sup>Z. M. Fang, A. Persson, and R. M. Cohen, *Phys. Rev. B* **37**, 4071 (1988).
- <sup>25</sup>G. L. Bir and G. E. Pikus, *Symmetry and Strain Induced Effects in Semiconductors* (Wiley, New York, 1974).
- <sup>26</sup>D. E. Aspnes, *Phys. Rev. B* **14**, 5331 (1976).
- <sup>27</sup>A. K. Saxena, *J. Phys. C* **13**, 4323 (1980).
- <sup>28</sup>B. Welber, M. Cardona, C. K. Kim, and S. Rodriguez, *Phys. Rev. B* **1**, 5729 (1975).
- <sup>29</sup>D. J. Wolford and J. A. Bradley, *Solid State Commun.* **53**, 1069 (1985).
- <sup>30</sup>M. Leroux, G. Neu, and V. Verié, *Solid State Commun.* **58**, 289 (1986).
- <sup>31</sup>M. Chandrasekhar, U. Venkateswaran, H. R. Chandraeskar, B. A. Vojak, F. A. Chambers, and J. M. Meese, in *Proceedings of the 18th International Conference on the Physics of Semiconductors, Stockholm, 1986*, edited by E. O. Engström (World Scientific, Singapore, 1987).
- <sup>32</sup>U. Venkateswaran, M. Chandrasekhar, H. R. Chandrasekhar, T. Wolfram, R. Fisher, W. T. Masselink, and H. Morkoç, *Phys. Rev. B* **31**, 4106 (1985).
- <sup>33</sup>See, for instance, M. Cardona and N. E. Christensen, *Phys. Rev. B* **35**, 6182 (1987).
- <sup>34</sup>C. Priester, G. Allan, and M. Lannoo, *Phys. Rev. B* **35**, 8519 (1988).
- <sup>35</sup>F. Minami, K. Todor, and K. Inoue, in *Proceedings of the International Conference on High Pressure in Semiconductor Physics, Tomasow, 1988* [*Semicond. Sci. Technol.* **4**, 265 (1989)].
- <sup>36</sup>H. Brooks, in *Advances in Electronics and Electron Physics*, edited by L. Morton (Academic, New York, 1955), Vol. 7, p. 85.
- <sup>37</sup>D. N. Mirlin, V. F. Sapega, I. Ya. Karlik, and R. Katilius, *Solid State Commun.* **61**, 799 (1987).
- <sup>38</sup>D. Scalbert, J. Cernogora, C. Benoît à la Guillaume, M. Maaref, F. F. Charfi, and R. Planel, *Solid State Commun.* (to be published).
- <sup>39</sup>H. Fritsche, *Phys. Rev.* **125**, 1560 (1962).
- <sup>40</sup>H. Mathieu, J. Camassel, and P. Merle, *Phys. Rev. B* **21**, 2466 (1980).
- <sup>41</sup>H. Mathieu, L. Bayo, J. Camassel, and P. Merle, *Phys. Rev. B* **22**, 4834 (1980).
- <sup>42</sup>J. Y. Marzin, in *Heterojunctions and Semiconductor Superlattices*, edited by G. Allan, G. Bastard, N. Boccaro, M. Lannoo, and M. Voos (Springer Verlag, Heidelberg, 1986), p. 161.
- <sup>43</sup>P. Lefebvre, Ph.D. thesis, Languedoc University of Science and Technology, Montpellier, 1988 (unpublished).
- <sup>44</sup>G. Danan, Ph.D. thesis, Université de Paris VI, 1988 (unpublished).